Bandgap closure and reopening in $CsAuI_3$ at high pressure

Shibing Wang,[1,2,*] Alexander F. Kemper,[2,3] Maria Baldini,[4] M. C. Shapiro,[5] Scott C. Riggs,[5] Zhao Zhao,[6] Zhenxian Liu,[7] Thomas P. Devereaux,[2,8] Ted H. Geballe,[5] Ian R. Fisher,[5] and Wendy L. Mao[1,8]

[1]*Department of Geological and Environmental Sciences, Stanford University, Stanford, California 94305, USA*
[2]*SIMES, SLAC National Accelerator Laboratory, Menlo Park, California 94025, USA*
[3]*Lawrence Berkeley National Laboratory, Berkeley, California 94720, USA*
[4]*HPSynC, Carnegie Institution of Washington, Washington, DC 20015, USA*
[5]*Department of Applied Physics and Geballe Laboratory for Advanced Materials, Stanford University, Stanford, California 94305, USA*
[6]*Department of Physics, Stanford University, Stanford, California 94305, USA*
[7]*Geophysical Laboratory, Carnegie Institution of Washington, Washington, DC 20015, USA*
[8]*Photon Science, SLAC National Accelerator Laboratory, Menlo Park, California 94025, USA*

(Received 27 February 2014; revised manuscript received 23 May 2014; published 9 June 2014)

Results of high-pressure infrared (IR) and Raman spectroscopy measurements are presented for the mixed valence compound $CsAuI_3$, where Au adopts Au^{I} and Au^{III} valency. Raman spectroscopy shows softening with pressure of the vibration modes in the Au^{III}-I_4 square planar units in the tetragonal phase, indicating a similar pressure-induced lattice distortion as found for the closely related compounds $CsAuCl_3$ and $CsAuBr_3$. Multiple features in the higher pressure spectra confirm that the high-pressure phase has a lower symmetry than the ambient pressure tetragonal structure, consistent with an orthorhombic structure discovered recently by x-ray diffraction measurements. From IR spectroscopy, we observed rapid bandgap closure at a rate of 0.2 eV/GPa in the tetragonal phase of $CsAuI_3$, close to the tetragonal-orthorhombic phase transition. The IR reflectivity shows a Drude-like behavior implying metallic conductivity. However, as the compound fully transforms to the orthorhombic phase, the bandgap reopens and the Drude behavior in the reflectivity disappears.

DOI: 10.1103/PhysRevB.89.245109 PACS number(s): 71.45.Lr, 78.30.Hv, 62.50.−p

I. INTRODUCTION

At ambient pressure, the family of $CsAuX_3$ (X = Cl, Br, or I) perovskites have a room temperature crystal structure with two distinct Au sites. The associated differences in coordination (both sites are octahedrally coordinated, but one with the two apical iodide ions significantly closer, and the other with equatorial iodide ions significantly closer) have led to a formal valence assignment $Au^{I}X_2$ and $Au^{III}X_4$. This state can be pictured as a local charge density wave (CDW) driven by charge disproportionation due to Jahn-Teller distortion [1].

Previous studies have revealed that the CDW state can be suppressed by high pressure [1,2]. The suppression of the CDW state corresponds to a mixed-valence (MV) to single-valence (SV) transition, where the charge disproportionation reduces to zero, and the electron configuration of both Au sites becomes $5d^9$ Au^{II}. Photoexcitation and application of pressure have been shown to induce the MV-SV transition in $CsAuX_3$. For $CsAuCl_3$, single-crystal x-ray diffraction studies show that its structure changes from tetragonal to cubic at 12.5 GPa [3], a completely symmetric structure with two crystallographically equivalent Au sites, which thus have the same electronic configuration. For $CsAuBr_3$, a careful refinement on the electron density of the higher pressure tetragonal phase suggests that it has already become single valence state at 8.1 GPa [4]. In addition, high-pressure Raman spectroscopy on $CsAuCl_3$ and $CsAuBr_3$ show that all observed vibrational modes disappear at 12.2 and 7.5 GPa respectively [5,6], consistent with the convergence of the Au^{I}-I and Au^{III}-I bond lengths in the SV state.

The MV-SV transition in $CsAuI_3$, however, remains unclear. In our latest study we found that in hydrostatic condition $CsAuI_3$ transitions from tetragonal to a lower symmetry orthorhombic phase [7], instead of a tetragonal phase with higher symmetry as previously claimed [2,8]. It was the higher symmetric tetragonal phase that was considered to be the direct evidence of the SV state. Moreover, a detailed high-pressure Raman spectroscopy study on the bonding of the iodide compound is lacking. How the lattice distortion and the CDW gap changes with pressure, as well as the electronic structure and optical properties of the higher pressure orthorhombic phase, remain unknown.

In this paper, we address these questions through a combination of high-pressure Raman spectroscopy and IR spectroscopy measurements. With the aid of density functional theory (DFT) calculations, we can assign the vibrational modes in $CsAuI_3$. We find that, in the tetragonal phase, the response of the lattice distortion to pressure, specifically in $Au^{III}I_4$ and $Au^{I}I_2$ units, is similar to the response in their chloride and bromide counter parts. We also observe that the CDW gap of $CsAuI_3$ decreases at a rate of 0.2 eV/GPa, and that a Drude-like behavior appears in the reflectivity spectra right at the transition pressure. The higher pressure orthorhombic phase, although with an odd number of electrons per unit cell, turns out to be an insulator with a finite gap at room temperature, as indicated by infrared spectroscopy.

II. EXPERIMENTAL AND THEORETICAL METHODS

$CsAuI_3$ crystals were grown by a self-flux method using CsI, Au, and I_2 as starting materials as described previously [9].

*shibingw@stanford.edu

In the Raman experiment, single-crystal chips with smooth and reflective surfaces were selected and loaded into a 150 μm diameter sample chamber inside a symmetric diamond anvil cell (DAC). The stainless steel gasket was precompressed between two diamonds with 500 μm culet diameter to a thickness of 60 μm. To maintain quasihydrostatic conditions at moderate pressure, silicone oil was chosen as the pressure transmitting medium, because the sample reacts with methanol-ethanol. In the IR experiment, the sample loading is similar except that a pair of type II diamonds were used, and Ne gas was loaded as a pressure medium using the gas loading system at GSECARS in the Advanced Photon Source, Argonne National Laboratory.

Room-temperature Raman spectra were collected using Raman systems in the Geophysical Laboratory, Carnegie Institution of Washington and in the Extreme Environments Laboratory at Stanford University in a backscattering geometry with an excitation wavelength of 514.5 nm. The energy resolution for all the spectra was 4 cm^{-1}. A set of polarizers were used for samples at ambient conditions to study the polarization dependence of the Raman features.

IR measurements were carried out on a Bruker Vertex 80v FT-IR spectrometer coupled to a Hyperion-2000 microscope with a MCT midband detector at beamline U2A of the National Synchrotron Light Source. Mid-IR measurements between 600 and 8000 cm^{-1} were performed using an internal source, while far-IR spectroscopy from 100 to 700 cm^{-1} utilized the synchrotron source [10].

A small ruby chip placed in the DAC was used for pressure calibration by observing the shift in the ruby R_1 fluorescence line [11]. Good hydrostaticity was maintained up to the highest pressures measured.

Density functional theory (DFT) calculations were performed using the QUANTUM ESPRESSO package [12]. We utilized fully relativistic projector augmented wave (PAW) pseudopotentials, and a plane-wave cutoff of 40 Ry. The calculations were performed on a $9 \times 9 \times 9$ momentum grid, which is sufficiently dense for convergence of the energies reported.

TABLE I. Raman modes associated with the iodine ions in tetragonal ($I4/mmm$) and orthorhombic ($Ibmm$) phases.

	Wyckoff sites	Coordinates				
$I4/mmm$						
Au^{III}	2a	(0,0,0)				
Au^{I}	2b	$(0,0,\frac{1}{2})$				
I(1)	8h	(x,x,0)	A_{1g}	B_{1g}	B_{2g}	E_g
I(2)	4e	$(\frac{1}{2},\frac{1}{2},z)$	A_{1g}			E_g
Cs	4d	$(0,\frac{1}{2},\frac{1}{4})$				
$Ibmm$						
Au	4a	(0,0,0)				
I(1)	8g	$(\frac{1}{4},\frac{1}{4},z)$	A_g	$2B_{1g}$	B_{2g}	B_{3g}
I(2)	4e	$(x,0,\frac{1}{4})$	A_g		B_{2g}	B_{3g}
Cs	4e	$(x,0,\frac{1}{4})$	A_g		B_{2g}	B_{3g}

III. RESULTS AND DISCUSSION

A. Raman spectroscopy

Similar to the chloride and bromide compounds in the $CsAuX_3$ (X = Cl, Br, and Al) family, $CsAuI_3$ adopts a tetragonal perovskite structure at ambient conditions (space group $I4/mmm$), with alternating elongated and compressed AuI_6 octahedra. One can also view the arrangement from a molecular point of view, and consider the compressed and elongated octahedra as dumbbell $Au^{I}I_2$ and square planar $Au^{III}I_4$ [Fig. 1(a)], a description used in previous Raman studies of $CsAuCl_3$ and $CsAuBr_3$ [5]. Based on site symmetry analysis, we list the Raman modes associated with all atoms in tetragonal $CsAuI_3$ in Table I. The system has two inequivalent I sites: the Raman modes associated with I(1) at (x, x, 0) are $A_{1g} + B_{1g} + B_{2g} + E_g$, and with I(2) at (1/2, 1/2, z) are $A_{1g} + E_g$.

In this work we use a combined experimental and theoretical approach to assign the Raman features. In the experiment setup, the incident laser polarization lies within the ab plane of the tetragonal crystal. Within point group D_{4h}, the transition rate for different vibrational modes with different laser polarization are listed in Ref. [13]. With parallel polarization

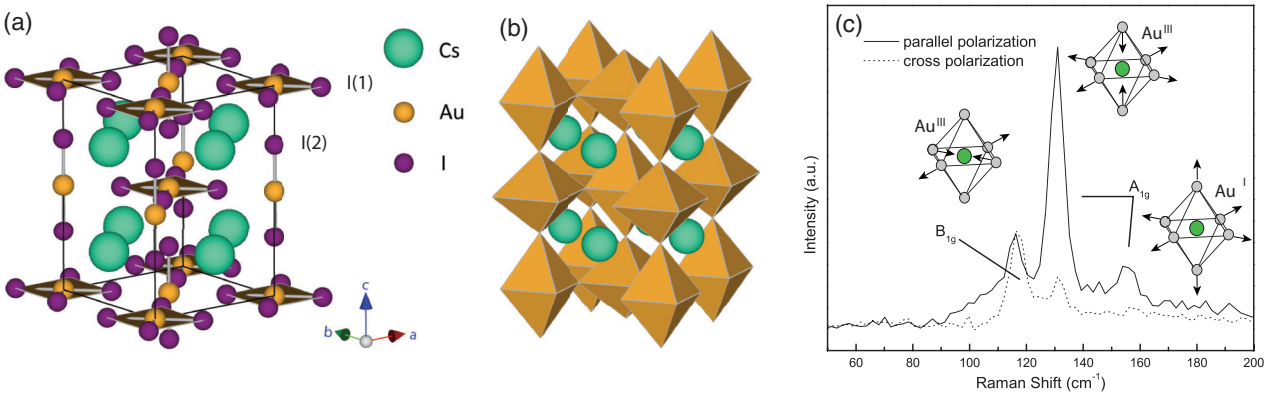

FIG. 1. (Color online) (a) Ambient pressure crystal structure of $CsAuI_3$ at 300 K, explicitly showing the linear square planar coordination of $Au^{I}I_2$ and $Au^{III}I_4$ respectively: I(1) as I^- associated with square planar $Au^{III}I_4$, and I(2) as I^- associated with linear $Au^{I}I_2$. (b) Crystal structure shown in alternating elongated and compressed AuI_6 octahedra, more clearly revealing the distorted perovskite structure. (c) Raman spectra of $CsAuI_3$ at ambient condition with different light polarization. The solid line represents parallel polarization, while the dashed line corresponds to cross-polarization. Schematics of the A_{1g} and B_{1g} vibrational modes are also presented.

TABLE II. Calculated Raman modes associated with the iodine ions at ambient pressure, 4.5 and 5.9 GPa, and experimentally measured vibrational frequency at ambient pressure, 1 and 5 GPa. Frequencies below 100 cm^{-1} are not observable due to the notch filter of Raman spectrometer.

		Computed			Experimental		
	Pressure	1 bar	4.5 GPa	5.9 GPa	1 bar	1 GPa	5 GPa
Mode 1 (cm^{-1})	A_{1g} (breathing)	152	177	182	157	162	174
Mode 2 (cm^{-1})	A_{1g}	103	87.8	27.7	135	132	121
Mode 3 (cm^{-1})	B_{1g}	78.8	72.1	25.8	120	117	108
Mode 4 (cm^{-1})	B_{2g}	70.1	84.9	89.1	N/A	N/A	N/A

$x'x'$ geometry or $c(a+b,a+b)\bar{c}$, the laser is sampling the A_{1g} and B_{2g} modes, while with cross polarization $x'y'$ geometry, or $c(a+b,a-b)\bar{c}$, the laser is sampling modes with B_{1g} and A_{2g} symmetry.

Raman spectra for $CsAuI_3$ at ambient conditions are displayed in Fig. 1(c). In our measurement, the incoming laser polarization is approximately along the $(a+b)$ direction. Therefore, peaks that are more intense with parallel polarization have the symmetry of A_{1g} or B_{2g}, while B_{1g} and A_{2g} will be more pronounced for cross polarization. For parallel polarization, three features are observed at 116, 131, and 157 cm^{-1}. For cross-polarization, the 116 cm^{-1} feature becomes much more pronounced; 131 cm^{-1} becomes significantly smaller; and the 157 cm^{-1} feature almost vanishes.

We identified the Raman active modes with DFT; the results are listed in Table II. At ambient conditions, we can predict four distinct modes above 50 cm^{-1} using calculations. Mode 1 has the highest frequency at 152 cm^{-1} and corresponds to a A_{1g}breathing mode of the AuI_6 octahedron, where all the I^- move in phase. The second highest frequency mode corresponds to a A_{1g}vibration that is similar to the octahedral breathing mode, but where the apical I^- are 180° out of phase with the planar I^-, i.e., more in line with a $Au^{I}I_2$ vibration. Mode 3 maps to a planar B_{1g}vibration where the x and y directions in the AuI_4 plane are 180° out of phase; see Fig. 1(b). Finally, the fourth mode corresponds to a B_{2g}planar motion where the I^- distort towards the empty site in the AuI square lattice (not shown in figure). Aside from the highest frequency A_{1g}mode, the calculated mode frequencies are lower than observed.

In the experimental spectra, we tentatively assign the 157 and 131 cm^{-1} features with A_{1g}, associated with I(1) and I(2) respectively [shown in Fig. 1(a)], which is consistent with the shorter Au^{I}-I(2) and longer Au^{III}-I(1) bonds (2.576 and 2.645 Å respectively) [9], similar to $CsAuCl_3$ and $CsAuBr_3$ [5]. The low-frequency mode at 116 cm^{-1} that is enhanced by cross polarization is assigned as the B_{1g}mode with I(1). These assignments will be further borne out by the pressure dependence of the phonon frequencies, whose tendency is correctly captured by calculations.

The evolution of $CsAuI_3$ Raman spectra with pressure is shown in Fig. 2. At 0.2 GPa, the Au^{III} A_{1g} and B_{1g} features are pronounced, and both of them shift to lower frequency with pressure up to 6.6 GPa. The spectra at 6.6 GPa shows a coexistence of the tetragonal and orthorhombic phase, consistent with the metastable kinetics of a first-order transition. At higher pressure, up to six new vibrational modes with much higher frequency emerge. These new Raman peaks disappear at 12.6 GPa, where the sample was reported to become disordered [7,8]. It is worth noting that, unlike in the tetragonal

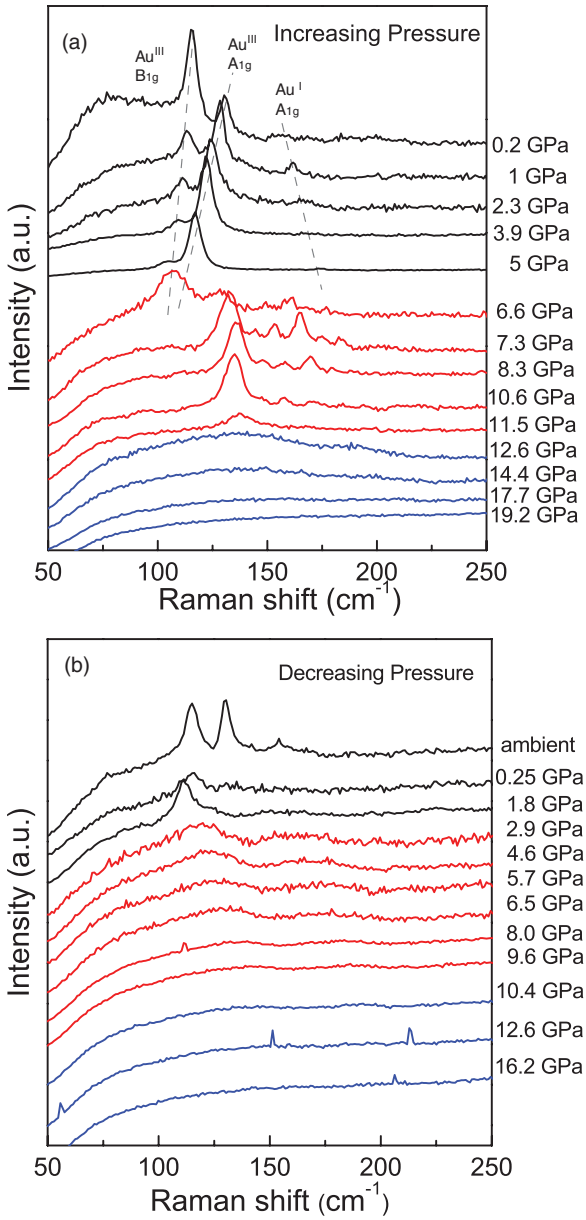

FIG. 2. (Color online) Raman spectra of $CsAuI_3$ during (a) compression and (b) decompression. Black represents tetragonal phase; red: orthorhombic; and blue: disordered. Details of the experimental geometry are described in the main text.

phases, the new Raman modes of the orthorhombic phase all shift to higher frequency with increasing pressure. We further took the Raman spectra of the compound while releasing pressure, and found that no features exist until 6.5 GPa. Below 6.5 GPa, broad features appear down to 2.9 GPa, and their frequency red-shifts as pressure is lowered, consistent with the features of the orthorhombic phase. Below 1.8 GPa, sharper features reemerge, and shift to higher frequency with lower pressure, indicating the crystalline tetragonal phase resumes at 1.8 GPa. This agrees with our previously reported x-ray diffraction data that the pressure-induced phase transition is a reversible first-order transition, with a large hysteresis [7].

According to previous Raman studies with polarized light on $CsAuCl_3$ and $CsAuBr_3$ [5], the B_{1g} and A_{1g} modes of Au^{III}-Cl_4 are only separated by 2 cm^{-1}, and the separation is 3 cm^{-1} for Au^{III}-Br_4 in $CsAuBr_3$. Therefore, only two distinct features are observed in the nonpolarized Raman spectra of $CsAuCl_3$ and $CsAuBr_3$ [5]. To compare the vibration of the different gold halide groups, we normalized the Raman frequencies by including the mass effect of the ions, $\nu_{\text{corr}} = \nu_{\text{measured}} \times \sqrt{\frac{m_1}{m_X}}$, $X = \text{Cl, Br}$ [6]. The mass-corrected Raman frequency for the A_{1g} and B_{1g} modes in $CsAuCl_3$ and $CsAuBr_3$ together with those measured in $CsAuI_3$ are displayed in Fig. 3. The mode with Au^{III}-X_4 shows a tendency towards lower frequencies for heavier ions, even if the weight information is already taken into account. Overall, the qualitative behaviors of the three modes are very similar for all three compounds: The lower frequency modes associated with Au^{III}-X_4 red-shift with pressure, while the higher frequency mode associated with Au^{I}-X_2 stiffens with pressure. The softening of the Au^{III}-X_4 mode can

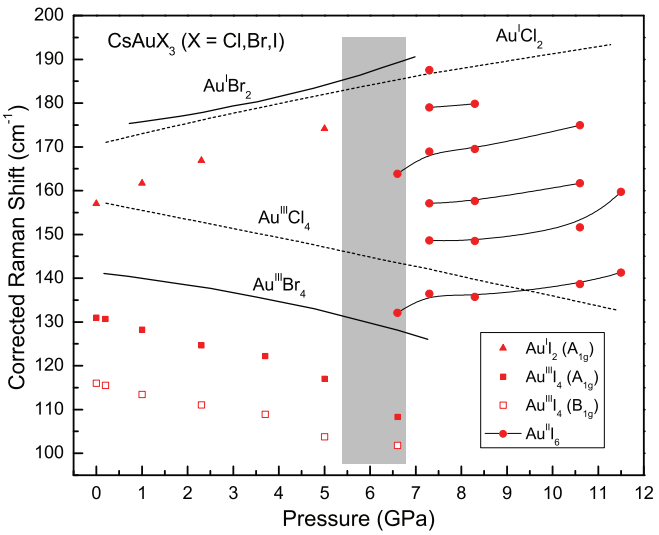

FIG. 3. (Color online) Raman modes of $CsAuI_3$ compared with mass-corrected modes of $CsAuCl_3$ and $CsAuBr_3$ as a function of pressure. The original Raman frequencies of $CsAuCl_3$ and $CsAuBr_3$ are from Ref. [5]. Dotted lines represent modes from Au-Cl units; solid lines from Au-Br units. Unfilled and filled squares are for the B_{1g} and A_{1g} modes of Au^{III}-I_4, and filled triangles are for the A_{1g} mode of Au^{I}-I_2 in the tetragonal phase. Filled circles stand for Raman modes in the iodide orthorhombic phase. The grey region indicates the pressure range of the first-order tetragonal-orthorhombic transition.

be understood by taking into account the structural effect of pressure-induced electron transfer from Au^{I} to Au^{III}; the Au^{III}-X_4 bond length increases as the anion moves towards (1/4, 1/4, 0), resulting in a less distorted Au^{III}-X_6, as evidenced by high-pressure x-ray studies [3,4]. The stiffening of the A_{1g} mode of Au^{I}-X_2 is suggested to be related to the hybridization of the $5d_{3z^2-r^2}$ state with the 6*s* state in the Au^{I} ion [5]. Overall, the Raman data at pressures lower than the structural phase transition show that the local distortion of AuI_6 octahedra in $CsAuI_3$ behaves similarly to $CsAuCl_3$ and $CsAuBr_3$, indicating that the compression of the tetragonal phase $CsAuX_3$ shares the same physics leading to the first-order structural phase transition.

We have previously proposed two different space groups *Ibmm* and *Immm* for the high-pressure phases from our earlier x-ray diffraction study [7]. The electronic configurations of the two structures are different: the one with space group *Ibmm* represents a single-valent Au, and *Immm* represents a mixed-valent Au. DFT calculations show that their energies are very close to each other (within approximately 50 meV after relaxation), but that the *Ibmm* structure is more energetically favorable. The Raman modes analyzed with relevant site symmetry in *Ibmm* are displayed in the lower part of Table I. The six modes we observed in the orthorhombic phase correspond to the enumeration of $2A_g + 2B_{1g} + 2B_{2g}$. As for *Immm*, the enumeration would have one more A_g mode coming from I(1) with coordinate $(x, y, 0)$.

The high-pressure SV $CsAuI_3$ is different from SV $CsAuCl_3$ and $CsAuBr_3$. The chloride and bromide SV phases are either cubic or near cubic in structure, and their Raman spectra show no first-order signal. As a result, the MV-SV transitions in $CsAuCl_3$ and $CsAuBr_3$ were determined by the disappearance of their Raman signal. In $CsAuI_3$, however, not only does the Raman signal not disappear at the pressure of the MV-SV accompanied structural transition (5.5–6 GPa), but the number of features increases. It is at even higher pressure, 12 GPa, where the orthorhombic phase becomes almost disordered [7] that the Raman signal disappears in $CsAuI_3$.

B. Infrared spectroscopy and reflectivity

IR spectroscopy can reveal the band-structure information on the compound. We measured high-pressure mid-IR transmission and reflectivity using an internal source, and far-IR transmission using the synchrotron source. We follow the procedures in a previously reported work to obtain the transmittance $T(\omega)$ and sample-diamond reflectivity $R^{SD}(\omega)$ (note that this is different from sample-air reflectivity) [14].

Figure 4 shows the transmittance and reflectance from 0.08 to 1 eV (610 to 8000 cm^{-1}). From the transmittance spectra, it is clear that the compound has a bandgap near 0.6 eV at 1.5 GPa [indicated by the red arrow in Fig. 4(a)] and the gap decreases with pressure until 4.8 GPa, at which pressure transmission of photons higher than 0.08 eV is significantly reduced. Meanwhile, the reflectivity increases with pressure up to 3.8 GPa, and then the spectral shape changes at 4.8 and 5.6 GPa. Specifically, a Drude-like mode appears in the 5.6 GPa spectrum. We fit the 5.6 GPa reflectivity spectrum using a method described in Ref. [15] which primarily is a Drude-Lorentz model taking into account the sample-diamond interface, with software REFFIT [16]. The original spectrum

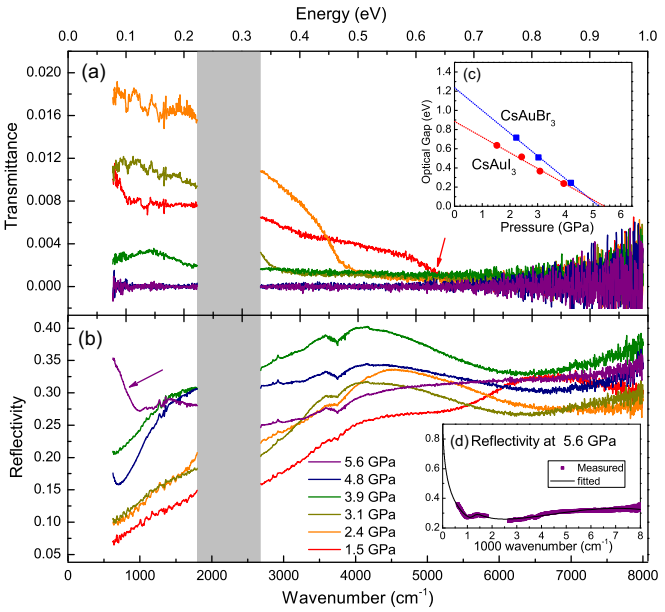

FIG. 4. (Color online) (a) Mid-IR transmittance and (b) $CsAuI_3$-diamond reflectivity below 5.6 GPa. The arrow in (a) points to the onset of the finite transmission signal. The arrow in (b) indicates the Drude-like mode observed for pressure at 5.6 GPa. (c) Fitted gap of tetragonal $CsAuI_3$ and $CsAuBr_3$ as a function of pressure (both obtained in this study). (d) Reflectivity spectrum at 5.6 GPa fitted with the Drude-Lorentzian model. The grey region is where diamond absorbs strongly.

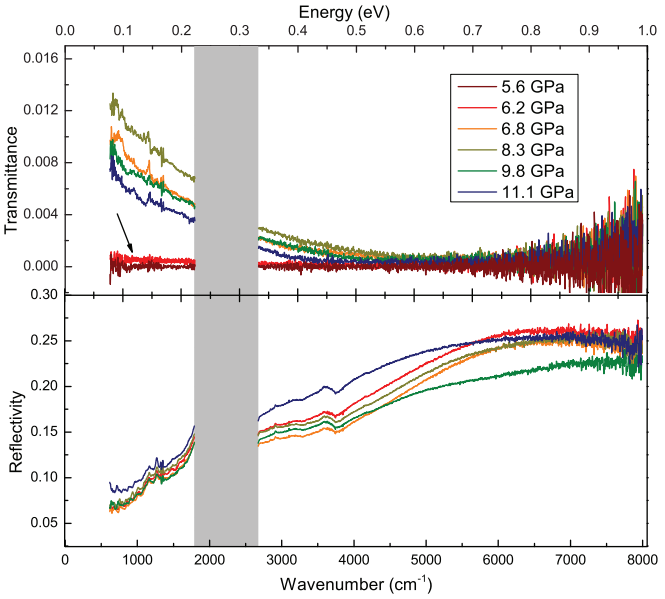

FIG. 5. (Color online) (a) Mid-IR transmittance and (b) $CsAuI_3$-diamond reflectivity above 5.6 GPa. The arrow in (a) points to the finite transmission through low wave numbers at 6.2 GPa. The grey region is where diamond absorbs strongly.

and the fitted spectum are shown in Fig. 4(d). The fitted Drude mode has a plasma frequency ω_p of 1.08×10^4 cm^{-1}; the fitted Lorentzian mode is centered at $\omega_0 = 1278$ cm^{-1}; χ^2 of the fitting is 1.9×10^3. The DC optical conductivity based on the Drude-Lorentzian fit is a bit less than 400 Ω^{-1}cm^{-1}. Previous transport measurement of $CsAuI_3$ on pressures lower than 4.7 GPa shows that the resistivity has metallic temperature dependence [1]. These raise the intriguing possibility that the material becomes a metal; however, without temperature dependence and a wider coverage of wave number in the far-IR region, we cannot unambiguously distinguish a true metallic state or a small gap semiconductor. It is worth mentioning again that, from our previous XRD study [7] we found that this pressure range is where the compound is undergoing a first-order structural phase transition, and there was coexistence of both phases at 5.9 GPa. It is very likely that at 5.6 GPa the high pressure orthorhombic phase starts to form.

The higher pressure spectra are shown in Fig. 5. The transmittance signal starts to reappear below 0.8 eV and increases as pressure increases to 8.3 GPa, indicating a new gap is opening at higher pressure. The intensity of transmission then decreases as pressure increases to 11 GPa. The shape of $T(\omega)$ spectra is also different. Before the structural phase transition (i.e., below 5.6 GPa), a clear step can be seen in the transmittance spectra. After the transition the long tail suggests the nature of the new bandgap is different from the CDW gap in the tetragonal phase. The reflectivity spectra are also different from those at pressures below 5.6 GPa: the low-energy (0.08–0.4 eV) reflectivity remains smaller than 0.17. This is consistent with the implication of the transmittance spectra that a bandgap opens up at pressure above 5.6 GPa. This nonmetallicity of the high-pressure single-valent phase of $CsAuI_3$ is in good agreement with previous transport measurements [8,17] and data from the photo-induced SV state reported in Ref. [18].

The shape of the transmission spectra in the tetragonal phase suggest the gap is close to a direct one. Therefore, we can estimate the bandgap from the onset of the transmission spectra, and plot the gap as a function of pressure in inset of Fig. 4. The bandgap energy changes linearly with pressure, and by extrapolation it closes at 5.4 GPa, very close to the pressure 5.6 GPa at which we observed a Drude-like behavior in the reflectivity spectrum. On the same figure we also plot the bandgap energy of $CsAuBr_3$ obtained in this study, and by extrapolation its bandgap also closes at approximately 5.2 GPa. Such a sensitive response (0.2 eV/GPa) of $CsAuI_3$ in the mid-IR region to pressure is likely to be a result of the CDW gap closure. The CDW gap is caused by the mixed valence of the Au^{I} and Au^{III} species, i.e., the inequivalent Au^{I}-I_6 and Au^{III}-I_6 octahedra. The closure of the gap indicates the negligible difference between the two octahedra, and therefore suggests the completion of the mixed-valence to single-valence transition. Such interpretation of the optical properties favors the *Ibmm* structure for the orthorhombic phase, which has two equivalent Au sites adopting the single-valent Au^{II} electronic configuration.

To study the optical behavior at even lower energy, i.e., close to the long-wavelength limit, and to compare with the Raman spectra, we measured the absorption of $CsAuI_3$ in the far-IR regime (10–80 meV), as shown in Fig. 6. In the tetragonal phase [Fig. 6(a)], the absorbance increases with pressure; i.e., the sample becomes progressively less transparent as pressure increases, indicating it is more reflective and has higher conductivity at these wave numbers. In the orthorhombic phase, the absorbance at 6.2 GPa is still large, but drops quickly

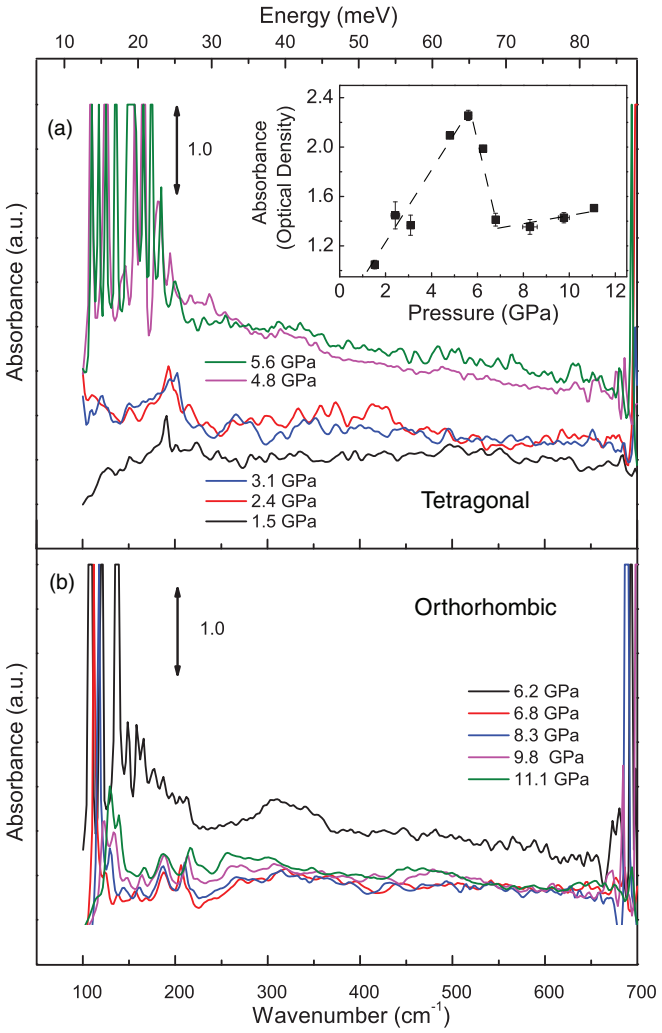

FIG. 6. (Color online) Far-IR absorption for tetragonal (a) and orthorhombic (b) structure as a function of pressure. Inset: Optical density of the $CsAuI_3$ sample at 400 cm^{-1} as a function of pressure; dashed lines are guides to the eyes.

at 6.8 GPa, and then gradually increases. This information is summarized in the inset of Fig. 6: the optical density at 400 cm^{-1} where no specific phonon features are observed is plotted as a function of pressure for $CsAuI_3$. It is clear that before the phase transition the sample absorbs more at 50 meV (400 cm^{-1}), while after the transition it becomes more transparent at this energy. The fact that the 5.6 GPa absorbance is still finite can be due to two reasons: first, the semiconducting orthorhombic phase has already formed at the pressure; second, the sample is thin (approximately 30–45 μm) compared to the far-IR wavelength, and allows light to transmit through. We also notice that there are 5–6 new IR bands between 100 and 300 cm^{-1} above 5.6 GPa in Fig. 6(b), which is consistent with the multiple (more than three) Raman features in the orthorhombic phase.

IV. CONCLUSIONS

Our Raman and infrared studies show that the electronic configuration and structure of $CsAuI_3$ undergo dramatic changes through the pressure-induced tetragonal to orthorhombic phase transition. We observed the closure of the CDW gap together with the structural transition, suggesting that the high-pressure orthorhombic phase is single valent and is composed of Jahn-Teller distorted $Au^{II}I_6$ octahedra, with Au $5d^9$ electronic configuration [7]. Mid-IR transmission spectra suggest that the gap of the orthorhombic phase is very different from the CDW gap in the tetragonal phase. A previous transport study speculated it is a Mott insulator [5], but more information is needed to clarify the nature of the insulating higher pressure phase. It also remains an open question whether any magnetic structure will emerge in single-valent $CsAuI_3$.

ACKNOWLEDGMENTS

The authors thank Dr. S. Tkachev for help with the gas loading system at the Advanced Photon Source. S.W., Z.Z., L.K., W.L.M., and T.P.D. are supported by Stanford Institute for Materials and Energy Science (DE-AC02-76SF00515). S.W. and M.B. are supported by EFree, an Energy Frontier Research Center funded by the US Department of Energy (DOE), Office of Science, Office of Basic Energy Sciences (BES) under Grant No. DE-SG0001057. M.C.S., S.C.R., T.H.G., and I.R.F. are supported by the Airforce Office of Scientific Research (AFOSR) under Grant No. FA9550-09-1-0583. The use of the U2A beamline was supported by the NSF (DMR-0805056; EAR 06-49658, COMPRES) and the DOE-NNSA (DE-FC03-03N00144, CDAC). NSLS is supported by the DOE/BES (DE-AC02-98CH10886).

[1] N. Kojima and N. Matsushita, Coord. Chem. Rev. **198**, 251 (2000).
[2] N. Kojima, Bull. Chem. Soc. Jpn. **73**, 1445 (2000).
[3] H. Matsushita, H. Ahsbahs, S. S. Hafner, and N. Kojima, J. Solid State Chem. **180**, 1353 (2007).
[4] M. Sakata, T. Itsubo, E. Nishibori, Y. Moritomo, N. Kojima, Y. Ohishi, and M. Takata, J. Phys. Chem. Solids **65**, 1973 (2004).
[5] X. J. Liu, Y. Moritomo, A. Nakamura, and N. Kojima, J. Chem. Phys. **110**, 9174 (1999).
[6] X. J. Liu, K. Matsuda, Y. Moritomo, A. Nakamura, and N. Kojima, Phys. Rev. B **59**, 7925 (1999).
[7] S. Wang, S. Hirai, M. C. Shapiro, S. C. Riggs, T. H. Geballe, W. L. Mao, and I. R. Fisher, Phys. Rev. B **87**, 054104 (2013).
[8] A. F. Kusmartseva, M. Yang, A. M. Arevalo-Lopez, K. V. Kamenev, and J. P. Attfield, Chem. Commun. (Cambridge) **46**, 6681 (2010).
[9] S. Riggs, M. Shapiro, F. Corredor, T. Geballe, I. R. Fisher, G. T. Mccandless, and J. Y. Chan, J. Cryst. Growth **355**, 13 (2012).
[10] Z. Liu, J. Hu, H. Yang, H. Mao, and R. Hemley, J. Phys.: Condens. Matter **14**, 10641 (2002).
[11] H. K. Mao, J. Xu, and P. M. Bell, J. Geophys. Res. **91**, 4673 (1986).
[12] P. Giannozzi *et al.*, J. Phys.: Condens. Matter **21**, 395502 (2009).

[13] T. P. Devereaux and R. Hackl, Rev. Mod. Phys. **79**, 175 (2007).
[14] X. Xi, C. Ma, Z. Liu, Z. Chen, W. Ku, H. Berger, C. Martin, D. B. Tanner, and G. L. Carr, Phys. Rev. Lett. **111**, 155701 (2013).
[15] H. Okamura, R. Kitamura, M. Matsunami, H. Sugawara, H. Harima, H. Sato, T. Moriwaki, Y. Ikemoto, and T. Nanba, J. Phys. Soc. Jpn **80**, 084718 (2011).
[16] A. B. Kuzmenko, REFFIT, available at http://optics.unige.ch/alexey/reffit.html.
[17] N. Kojima, H. Hasegawa, H. Kitagawa, T. Tikegawa, and O. Shimomura, J. Am. Chem. Soc. **116**, 11368 (1994).
[18] M. Trigo, J. Chen, M. P. Jiang, W. L. Mao, S. C. Riggs, M. C. Shapiro, I. R. Fisher, and D. A. Reis, Phys. Rev. B **85**, 081102(R) (2012).